CrossMark

Finite Element Stereo Digital Image Correlation: Framework and Mechanical Regularization

J.-E. Pierré[1] · J.-C. Passieux[1] · J.-N. Périé[1]

Abstract The use of Finite Element meshes in Digital Image Correlation (FE-DIC) is now widespread in experimental mechanics but, so far, FE have been much less used in Stereo-DIC. The first goal of this paper is to explain in detail how to use FE in Stereo-DIC by means of a formulation in the world coordinate system. More precisely, the paper describes how to calibrate possibly non-linear model of cameras and to measure shapes and displacements with an FE mesh. It also shows that, with such a framework, it is possible to regularize the measurement with an FE model based on the same mesh. For instance, using this technique, it is possible to measure the rotation field of a bending plate in addition to its displacement.

Keywords Digital image correlation · Stereovision · Finite element · Mechanical regularization · Plate kinematics

Introduction

Digital Image Correlation (*DIC*) and Digital Volume Correlation (*DVC*) [6, 11, 24] are now widely used in experimental mechanics. These families of methods are intended to measure 2D or 3D displacement fields from digital planar or volume images, respectively. In their initial version, the idea was to search for the best parameters of a given transformation to register small independent subsets of pixels.

✉ J.-C. Passieux
passieux@insa-toulouse.fr

[1] Institut Clément Ader, CNRS UMR 5312, Université Fédérale Toulouse Midi-Pyrénées, INSA/UPS/Mines Albi/ISAE – 3 rue Caroline Aigle, 31 400 Toulouse, France

In the context of experimental mechanics, the use of Finite Elements in the framework of DIC/DVC (*FE-DIC/DVC* [2, 23]) has been extensively developed during the last decade. Among the many advantages of this technique, the main interest for the present work lies in the fact that it provides a very simple bridge between experiments and simulations, which is very convenient for validation [16] and identification purposes [9, 14, 19] and for performing mechanically regularized measurements.

Even in situations where 2D-DIC could be used, Stereo-DIC is preferred for both its accuracy and its simplicity [5, 25]. Classically, the idea of Stereo-DIC is to use one stereoscopic image pair, f_1 and f_2, in a reference configuration at t_0 and a second pair, g_1 and g_2, at $t_0 + dt$ in a deformed configuration, see Fig. 1.

The classical Stereo-DIC procedure involves a chain of optimization problems:

|	
Calibration:	1) find ex/in-trinsic parameters from a set of images of calibration grids
Shape Measurement:	2) find matching field $\mathbf{d}$ between reference images f_1 and f_2
	3) triangulation: find $\mathbf{X}$ at t_0 from $\mathbf{x}_1$ and $\mathbf{x}_2 = \mathbf{x}_1 + \mathbf{d}(\mathbf{x}_1)$
Displacement Measurement:	4) find matching $\mathbf{t}$ between images f_1 and g_1
	5) find matching $\mathbf{t}'$ between images f_1 and g_2
	6) triangulation: find $\mathbf{X}$ at $t_0 + dt$ from $\mathbf{x}'_1 = \mathbf{x}_1 + \mathbf{t}(\mathbf{x}_1)$ and $\mathbf{x}'_2 = \mathbf{x}_1 + \mathbf{t}'(\mathbf{x}_1)$

Eventually, the 3D displacement is estimated by comparing measured shapes: $\mathbf{U} = \mathbf{X}' - \mathbf{X}$. The drawback of this classical Stereo-DIC formulation is that the displacement is

Fig. 1 Main steps of a 3D displacement field measurement of a surface with classical Stereo-Digital Image Correlation. Pairings are in *green* and triangulations in *blue*
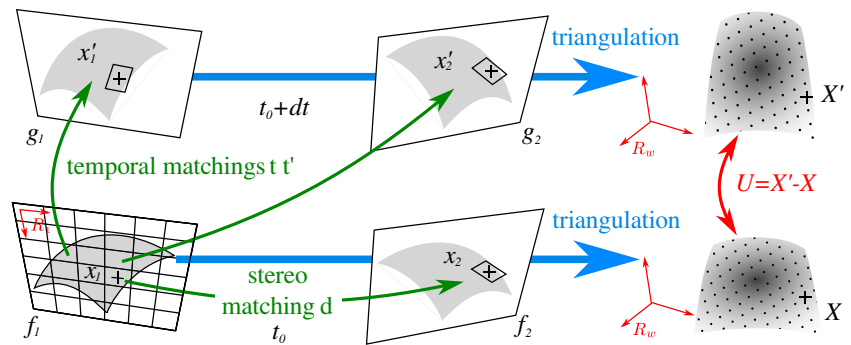
not the unknown of a single optimization problem as it is the case with 2D-DIC and DVC. In this situation, the bridge between measurement and simulation is less direct. In particular, it is not possible to apply mechanical regularization in this framework.

In contrast to that on DIC and DVC, the literature on FE-Stereo-DIC (or FE-SDIC) is much less prolific - certainly because the extension is not straightforward. The first attempt was proposed in [22], where a theoretical FE mesh was used to provide the displacement measurement solution to one single problem defined in the world coordinate system. In [22], this formulation is not fully exploited since it is not used for calibration and shape measurement. A very similar global stereo formulation based on IsoGeometric Analysis (*IGA*) was proposed in [1, 3]. It is used not only for the displacement measurement but also for the calibration of a linear camera model and shape measurement.

In the present paper, we develop and give a detailed description of a general framework covering all the aspects of FE-Stereo-DIC. It consists of a formulation in the world coordinate system that makes it possible to calibrate a stereo rig (with possibly non-linear camera models), to measure the actual shape of the specimen and to measure the displacement field, using an FE interpolation. A technique is proposed for building the minimal number of integration points in this context. In addition, it becomes possible to add a regularization based on an FE mechanical model. For instance, the method is illustrated with a measurement of the kinematic fields of a bending plate; in this case, the

meaning of kinematic field includes not only displacements but also rotations.

In "Rewriting the Stereo-DIC Problem in the World Coordinate System with Finite Elements" the three problems of calibration, shape measurement and displacement measurement will be rewritten as three optimization problems where the unknowns are the intrinsic/extrinsic parameters, the shape, and the 3D displacement. Then, in "Stereo-DIC and Plate Regularization (R-FE-SDIC)", it will be shown that, with the proposed framework, it is possible to directly add a constraint of regularity such as a mechanical regularization term. It will also be shown that the use of a plate model in the regularization is likely to provide accurate rotation fields. Finally in "Application", both a synthetic and a real test case will be presented in order to illustrate the efficiency of the method, the effects of the parameters, and the method's robustness with respect to noise.

Rewriting the Stereo-DIC Problem in the World Coordinate System with Finite Elements

This section contains the three parts of the measurement of a 3D displacement in the reference system R_W described by the mesh. With an FE mesh, the theoretical shape does not necessarily correspond to the real one. Therefore, a displacement measurement needs two preliminary steps (Fig. 2).
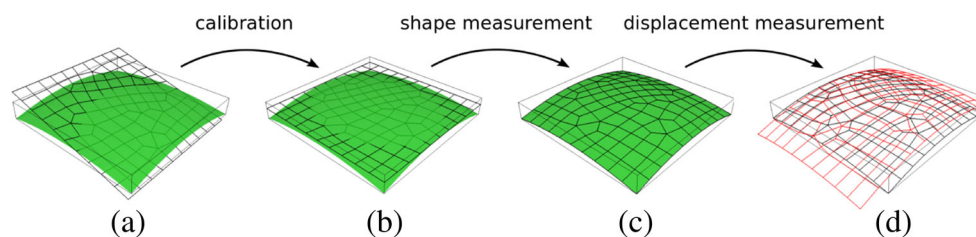
Fig. 2 Steps of the new Stereo-DIC formulation with a Finite-Element mesh (FE-SDIC): (**a**) first guess of the theoretical CAD mesh plate (*black*) on the real (*a priori* unknown) plate (*green*) before any calibration or shape measurement. (**b**) Calibration of the extrinsic parameters by DIC (with fixed 3D points **X**). (**c**) Shape measurement (with fixed parameters $\mathbf{p}_c$). (**d**) Temporal measurement of the 3D displacement **U** (from the *black* position of the mesh to the *red* one)

Firstly, cameras have to be located in the world coordinate system. This is called the **extrinsic parameters calibration** but **intrinsic parameters** can also be optimized according to the mesh used ("Calibration of Extrinsic and Intrinsic Parameters"). Then, the mesh shape has to be corrected: the projections of each point of the mesh in the two cameras (with their projectors $\mathbf{P}_c$) have to be stereo-matched (the corresponding grey-levels must be equal). This is the **shape measurement** step ("Shape measurement with an FE mesh"). A very similar approach has already been published in [1] for a CAD-based shape measurement with NURBS. Finally, the **3D displacement** between two steps can be measured ("3D displacement measurement").

Calibration of Extrinsic and Intrinsic Parameters

In this study, since the method is based on a Gauss-Newton algorithm, the calibration has to be initialized with the Stereo Software Vic-3D^{TM}. The calibration consists of finding all parameters $\mathbf{p}_c$ of each camera's projector $\mathbf{P}_c$:

– Six **extrinsic parameters** in order to find the position of the camera's reference system in R_W : three translations and three rotations.
– Four **linear intrinsic parameters** in order to project a point from the camera to its image : two focal lengths (f_u, f_v) and two centres of image (c_u, c_v) along the horizontal, u, and vertical, v, directions.

– At least **two non-linear intrinsic parameters** : the first order of radial distortion κ and the *skew* angle.

More details on the non-linear models of cameras can be found in [5, 17]. In this paper, the intrinsic parameters are initialized with Vic-3D^{TM}. The first problem is to find the extrinsic parameters in order to locate the 3D Finite Element mesh (considered rigid) as close as possible to the real surface, which is unknown. In the following, $\mathbf{p}_c$ denotes the extrinsic parameters of the projector $\mathbf{P}_c$ associated with the image f_c (the intrinsic parameters are fixed). For the sake of simplicity, we first consider a standard stereo bench, *i.e.* $c = \{1; 2\}$. The parameters $\mathbf{p}_c$ are assessed by minimizing the following objective functional based on the grey-level conservation assumption:

$$\mathbf{p}_1^\star, \mathbf{p}_2^\star = \underset{\mathbf{p}_1, \mathbf{p}_2}{\arg\min} \ \int_\Omega \Big[f_1 \left(\mathbf{P}_1(\mathbf{X}, \mathbf{p}_1) \right) - f_2 \left(\mathbf{P}_2(\mathbf{X}, \mathbf{p}_2) \right) \Big]^2 d\mathbf{X} \tag{1}$$

where $\mathbf{X}$ stands for a 3D point located on the visible surface, Ω, of the specimen.

As mentioned previously, the quadrature is performed in the 3D domain and one image is not preferred over another (there is no concept of master-slave), each camera being treated symmetrically. This non-linear problem is solved with a Newton algorithm. At iteration k, parameters $\mathbf{p} = [\mathbf{p}_1, \mathbf{p}_2]^T$ are sought in the form $\mathbf{p}^{k+1} = \mathbf{p}^k + \delta\mathbf{p}$. After linearization and differentiation, the problem reads:

$$\mathbf{M}_{ext}^k \ \delta\mathbf{p} = \mathbf{b}_{ext}^k$$

$$\begin{cases} M_{ext,ij}^k = \int_\Omega \left(\frac{\partial \mathbf{P}_1}{\partial p_i} \nabla f_1 - \frac{\partial \mathbf{P}_2}{\partial p_i} \nabla f_2 \right) \left(\frac{\partial \mathbf{P}_1}{\partial p_j} \nabla f_1 - \frac{\partial \mathbf{P}_2}{\partial p_j} \nabla f_2 \right)^T d\mathbf{X} \\ \mathbf{b}_{ext,i}^k = -\int_\Omega \left(\frac{\partial \mathbf{P}_1}{\partial p_i} \nabla f_1 - \frac{\partial \mathbf{P}_2}{\partial p_i} \nabla f_2 \right) \left(f_1 \left(\mathbf{P}_1(\mathbf{X}, \mathbf{p}_1^k) \right) - f_2 \left(\mathbf{P}_2(\mathbf{X}, \mathbf{p}_2^k) \right) \right) d\mathbf{X} \end{cases}$$

where $\frac{\partial \mathbf{P}_c}{\partial p_i}$ are the projectors $\mathbf{P}_c$ gradient with respect to the extrinsic parameters (even with a non-linear model, an analytical expression is known). ∇f_c is image f_c gradient at $\mathbf{P}_c(\mathbf{X}, \mathbf{p}_c^k)$ which depends on $\mathbf{p}_c$. This means that the operator $\mathbf{M}_{ext}^k$ has to be re-assembled at each iteration.

For a gradient algorithm, the initial guess should be close to the solution. The first guess can be obtained "by hand" by selecting some points in each image and on the mesh. (It would also be possible to detect at least three particular points with a pattern recognition algorithm.) Then, a small non-linear problem has to be solved. This problem has the same expression as the bundle adjustment (2) [28] but, here, $\mathbf{X}$, $\mathbf{x}_1$, $\mathbf{x}_2 = \mathbf{x}_1 + \mathbf{d}(\mathbf{x}_1)$ are fixed and only the extrinsic parameters are sought:

$$\mathbf{p}_1^\star, \mathbf{p}_2^\star = \underset{\mathbf{p}_1, \mathbf{p}_2}{\arg\min} \ \| \mathbf{P}_1(\mathbf{X}, \mathbf{p}_1) - \mathbf{x}_1 \|_2^2 + \| \mathbf{P}_2(\mathbf{X}, \mathbf{p}_2) - \mathbf{x}_1 - \mathbf{d}(\mathbf{x}_1) \|_2^2 \tag{2}$$

In order to illustrate these steps, Fig. 2(a) shows the first guess of the position of the mesh on the real surface. Figure 2(b) is the situation after the extrinsic calibration (equation (1)). In these two steps, the mesh $\mathbf{X}$ is considered fixed in its reference system and the goal is to position this system as close as possible to the unknown surface by finding the rigid translations and rotations.

In *ref.* [1], some intrinsic parameters of linear camera models are estimated using the same framework (using the speckle pattern of the specimen only). However, the measurement of a least one distance is needed to obtain an absolute estimate of, for instance, the focal length. Here, the model of the camera is more complex (non-linear with distortions) and the initial mesh is flat. Thus, intrinsic parameters cannot be optimized at the same time as the extrinsic ones. The idea would be to release all intrinsic parameters once the extrinsic are optimized. The functional

is the same (equation (1)) but with $\mathbf{p}_c$ containing only intrinsic parameters ($c_u, c_v, f_u, f_v, \kappa, skew$) (the extrinsic parameters are now fixed). It is possible to iterate these optimizations alternately.

In practice, and in order to be more generic, we decided to calibrate the intrinsic parameters using classic planar calibration targets. This step was achieved using Vic-3D$^{\text{TM}}$. It was verified that these parameters were very close to the local minimum of the above grey-level-based functional.

Shape measurement with an FE mesh

Once all the cameras' parameters $\mathbf{p}_c$ are known (and optimized), the shape has to be corrected. Measuring the shape means finding the position $\mathbf{X}$ that verifies grey-level conservation. Here, it is verified between the reference images of the two cameras . The method used is the same as for the camera parameters but the unknowns are the 3D positions $\mathbf{X}$:

$$\mathbf{X}^\star = \arg\min_{\mathbf{X}} \int_\Omega \left[f_1\left(\mathbf{P}_1(\mathbf{X}, \mathbf{p}_1)\right) - f_2\left(\mathbf{P}_2(\mathbf{X}, \mathbf{p}_2)\right) \right]^2 d\mathbf{X} \tag{3}$$

At iteration k, the estimate of the position is written $\mathbf{X}^{k+1} = \mathbf{X}^k + \delta\mathbf{X}$, where the displacement correction $\delta\mathbf{X}$ is sought in the finite element subspace with $\delta\mathbf{X} = \sum_i \mathbf{N}_i(\mathbf{X})q_i$:

$$\mathbf{M}_{shape}^k \mathbf{q} = \mathbf{b}_{shape}^k$$

$$\begin{cases} \mathbf{M}_{shape,ij}^k = \int_\Omega \mathbf{N}_i^T \left(\nabla\mathbf{P}_1\nabla f_1 - \nabla\mathbf{P}_2\nabla f_2\right)\left(\nabla\mathbf{P}_1\nabla f_1 - \nabla\mathbf{P}_2\nabla f_2\right)^T \mathbf{N}_j \, d\mathbf{X} \\ \mathbf{b}_{shape,i}^k = -\int_\Omega \mathbf{N}_i^T \left(\nabla\mathbf{P}_1\nabla f_1 - \nabla\mathbf{P}_2\nabla f_2\right)\left(f_1\left(\mathbf{P}_1(\mathbf{X}^k, \mathbf{p}_1)\right) - f_2\left(\mathbf{P}_2(\mathbf{X}^k, \mathbf{p}_2)\right)\right) d\mathbf{X} \end{cases}$$

where $\nabla\mathbf{P}_c$ are the projectors' spatial gradients which have an analytical form. As for the calibration, the operator $\mathbf{M}_{shape}^k$ has to be re-assembled at each iteration. After convergence, an estimate of the real shape is obtained (see Fig. 2(c)).

Remarks:

– Since this is based on a Gauss-Newton algorithm, the algorithm requires an initialization step. Usually, a multigrid initialization with pixel aggregation (coarse graining) is used [18]. However, unlike what is usually done in 2D-DIC, where this step is carried out with a coarse mesh, here the same mesh is used with a decreasing Tikhonov regularization in order to avoid 3D projection of fields from one mesh to another.

– As noted previously, $\mathbf{M}_{shape}^k$ has to be re-assembled at each iteration. This induces a significant cost because, here, the reference images of all cameras are compared by pairs. For n cameras, there are $\frac{n(n-1)}{2}$ pairs of cameras. On the other hand, in [4], a reference object $\hat{f}$ with an intrinsic texture is created, and all images are compared to $\hat{f}$, which is faster when the number of cameras is four or more because only n pairs are considered.

Regularization As always in DIC, this problem is ill-posed. With the classical approach, there are two unknowns (the components of the left-right disparity field, $\mathbf{d}$, on the image) for only one scalar equation (grey-level conservation). Here, a 3D field is sought, which means that, for the same number of equations, there is one more unknown. In problem (3), the mesh can slide along the surface of the object. There can be global sliding (see Fig. 3(b)) which implies that the dimension of the operator's kernel is at least 3 (sliding along two surface directions and one rotation). But in the formulation, the problem is even harder because each node can move relatively to another (see Fig. 3(c)) without changing the value of the functional. Thus, a higher degree of regularization has to be added to the functional.

For the local sliding, an isometric constraint can be imposed, like a Tikhonov regularization term:

$$\begin{aligned} \delta\mathbf{X}^\star = \arg\min_{\delta\mathbf{X}} \int_\Omega &\left[f_1(\mathbf{P}_1(\mathbf{X} + \delta\mathbf{X}, \mathbf{p}_1)) \right. \\ &\left. - f_2(\mathbf{P}_2(\mathbf{X} + \delta\mathbf{X}, \mathbf{p}_2)) \right]^2 d\mathbf{X} + \lambda \, \|\delta\mathbf{X}\|_{\mathbf{K}}^2 \end{aligned}$$

where the norm $\|\cdot\|_{\mathbf{K}}$ can be associated with a mechanical operator $\mathbf{K}$ (truss, stiffness or Laplace). One advantage of using SDIC with NURBS [1] is that only a few control points are necessary to describe a surface that indirectly regularizes the problem. So the shape interpolation can be uncoupled from the displacement interpolation, which can be refined without modifying the shape. In FE, this uncoupling is not possible and the same mesh is used for both shape and displacement measurement. Thus, it must be regularized externally.

However, both NURBS and FE approaches are subject to global sliding. The previous regularization does not prevent that problem. These shifts are particularly visible when iterating alternately between the optimization of the camera parameters and the shape measurement.

To avoid these shifts and restore the uniqueness of the problem, it was decided to seek the correction of the nodal

Fig. 3 Illustration of the ill-posed problem of shape measurement. (**a**) Theoretical position of the mesh after calibration and shape measurement. (**b**) Global or (**c**) Local sliding during the shape measurement

(a)　　　　　　　(b)　　　　　　　(c)
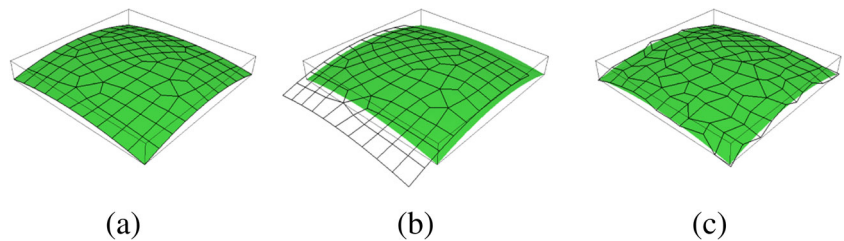
displacement along the normal to the surface [13]. The problem then has only one degree of freedom (*dof*) per node. In practice, the surface normal is estimated at each node (average of the neighbouring element normals) in the initial shape of the mesh.

3D displacement measurement

Once the real shape (thus, the real mesh) is known, it is possible to measure the 3D displacement $\mathbf{U}$ between two steps (t_0 and $t_0 + dt$). Unlike classical Stereo-DIC, the three optimisation problems are turned into a single problem where $\mathbf{U}$ is the only unknown. The main idea for this reformulation is to work only in the 3D mesh, chosen to be the world coordinate system R_W. All problems are written in this 3D coordinate system and weak-form integrals of the grey-level conservation are also in R_W.

For each 3D point $\mathbf{X}$, the projector $\mathbf{P}_c$ gives a point $\mathbf{x}$ in the image. Obviously, it is also possible to have the projection of the displaced point $\mathbf{X}' = \mathbf{X} + \mathbf{U}(\mathbf{X})$ (at $t_0 + dt$) in the images of the deformed configuration g_c (see Fig. 4).

The point $\mathbf{X}$ is projected on the reference image f_c and $\mathbf{X}'$ is projected on the image g_c. Their grey-levels should be equal for each camera c. Thus, the functional reads:

$$\mathbf{U}^\star = \underset{\mathbf{U}}{\arg\min} \sum_c \int_\Omega \Big[f_c\left(\mathbf{P}_c(\mathbf{X}, \mathbf{p}_c)\right) \\ - g_c\left(\mathbf{P}_c(\mathbf{X} + \mathbf{U}(\mathbf{X}), \mathbf{p}_c)\right) \Big]^2 d\mathbf{X} \quad (4)$$

which is just the grey-level conservation equation for each camera. This corresponds to the vertical pairing in Fig. 4. Each term of each camera being independent, it is possible

Fig. 4 3D displacement measurement in Stereo-DIC with a finite element based method (FE-SDIC)
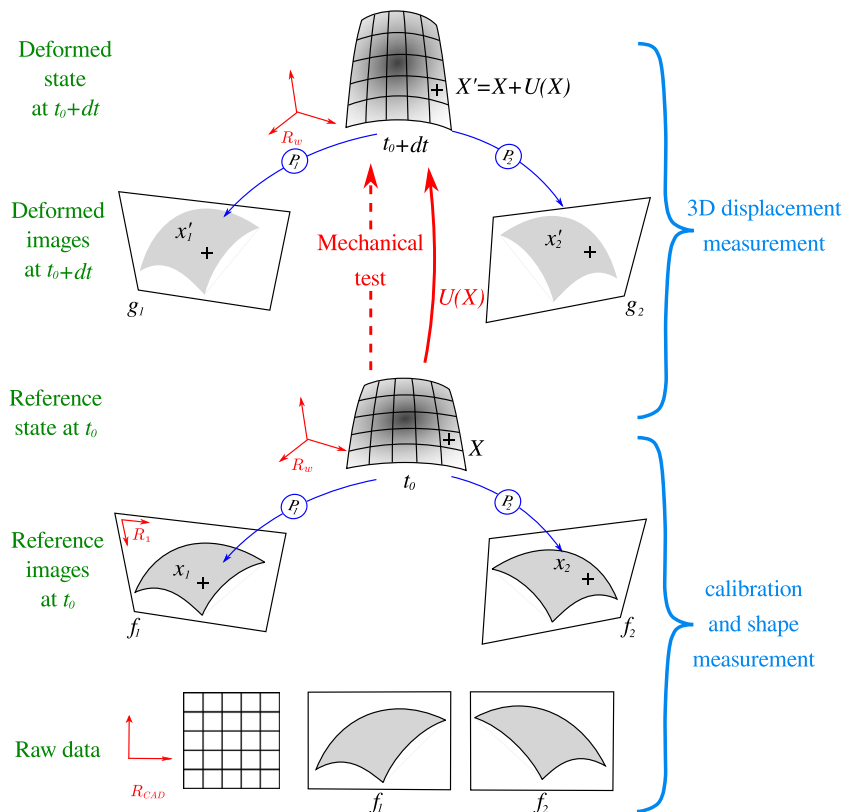
to consider more than two cameras [4]. Such a formulation in the world coordinate system was first introduced in [22]. The benefit is that each camera is used symmetrically. At iteration k, a correction of the 3D displacement field is introduced: $\mathbf{U}^{k+1} = \mathbf{U}^k + \sum_i \mathbf{N}_i(\mathbf{X})q_i$ and the problem reads:

$$\underbrace{\left(\sum_c \mathbf{M}_{dic}^{c,k}\right)}_{\mathbf{M}_{stereo}^k} \mathbf{q} = \underbrace{\left(\sum_c \mathbf{b}_{dic}^{c,k}\right)}_{\mathbf{b}_{stereo}^k}$$

$$\begin{cases} \mathbf{M}_{dic,ij}^{c,k} = \int_\Omega \mathbf{N}_i^T (\nabla \mathbf{P}_c \nabla f_c)(\nabla \mathbf{P}_c \nabla f_c)^T \mathbf{N}_j d\mathbf{X} \\ \mathbf{b}_{dic,i}^{c,k} = \int_\Omega \mathbf{N}_i^T (\nabla \mathbf{P}_c \nabla f_c) \left(f_c(\mathbf{P}_c(\mathbf{X}, \mathbf{p}_c)) - g_c(\mathbf{P}_c(\mathbf{X} + \mathbf{U}^k, \mathbf{p}_c))\right) d\mathbf{X} \end{cases}$$

Remarks:

– Both the left and right hand sides are sums of the independent operators on each camera. This implies that this problem can be parallelized as in the domain decomposition method in 2D-DIC [15].
– Like shape measurement, this algorithm needs an initialization step, such as a multigrid initialization based on pixel aggregation (coarse graining), and a Tikhonov regularization with a Laplacian operator.
– The correlation operator $\mathbf{M}_{stereo}^k$ depends on the displacement (because of the gradient of the projectors $\nabla \mathbf{P}_c(\mathbf{X} + \mathbf{U}^k)$), which means once again that it should be re-assembled at each iteration. In practice, this is not done because the multigrid initialization is close to the actual displacement. Thus, no significant difference is found between the situations with or without re-assembling (except that the former is far more time consuming).

To avoid a time drift of the pairing, it is also possible to introduce an additional term that minimizes the difference of grey-level between the images of the deformed configuration g_c at $t_0 + dt$ taken in pairs (this corresponds to a horizontal pairing in Fig. 4):

$$\mathbf{U}^\star = \underset{\mathbf{U}}{\arg\min} \sum_c \int_\Omega \left[f_c(\mathbf{P}_c(\mathbf{X}), \mathbf{p}_c) - g_c(\mathbf{P}_c(\mathbf{X} + \mathbf{U}(\mathbf{X}), \mathbf{p}_c)) \right]^2 d\mathbf{X}$$
$$+ \sum_c \sum_{e<c} \int_\Omega \left[g_c(\mathbf{P}_c(\mathbf{X} + \mathbf{U}(\mathbf{X}), \mathbf{p}_c)) - g_e(\mathbf{P}_e(\mathbf{X} + \mathbf{U}(\mathbf{X}), \mathbf{p}_c)) \right]^2 d\mathbf{X}$$

(5)

The pairing at t_0 is already verified with the calibration and the shape measurement. Of course, with this last term, a non-negligible cost is added when more than two cameras are used.

Quadrature In all the previous equations, quadrature was performed in the 3D world coordinate system and not on

the images as with classical DIC. So a dedicated quadrature method had to be set up. In contrast to simulation where a Gauss method is efficient, here, the integrand involves the greyscale gradient, which has a very short variation length. A Riemann integral method was therefore chosen by splitting each finite element homogeneously and homothetically. This choice has been proven to be more accurate [17]. In practice, a smaller number of points can be built with equivalent accuracy. This method considers an inhomogeneous partition of quadrangles and triangles in the isoparametric coordinate system, built by homogeneous partition of the two smallest edges. In Fig. 5, we show that such a technique significantly reduces the number of integration points. According to our tests, with this method, there is rarely more than one integration point per pixel.

Remark In this work, this formulation in the 3D coordinate system is needed in order to add a mechanical regularization term to the Stereo-DIC measurement. However, this is also interesting in 2D-DIC [17] for two reasons:

– The pixel based quadrature does not integrate a constant function accurately. The area of an element is approximated by an integer number of pixels and depends on the point of view of the camera. Even the shapes of the elements are not accurate because of the linear approximation of the element edges: with distortions the projection of a segment is not necessarily linear. This has little impact on the standard uncertainty of the measurement but can improve the systematic bias by an order of magnitude, even with a simple linear model of the camera.
– A more complex model of the camera with distortions can be used which drastically decreases measurement uncertainties. This is useful when identifying parameters with a FEMU method based on displacement (FEMU-U). It is also an essential method for crack propagation based on Williams series if it is not possible to use a telecentric lens.

Stereo-DIC and Plate Regularization (R-FE-SDIC)

Once the 3D displacement is the only unknown, it is easier to add a regularization term. The idea is not only to make a measurement, but also to filter it with a mechanical model. This is very important when trying to measure rotation fields accurately.

Furthermore, for a plate or shell model, not only displacements but also rotations at the mid-surface are considered (see Fig. 6). The 3D displacement, $\mathbf{U}$, measured with Stereo-DIC is the displacement of the observed surface, *i.e.* the
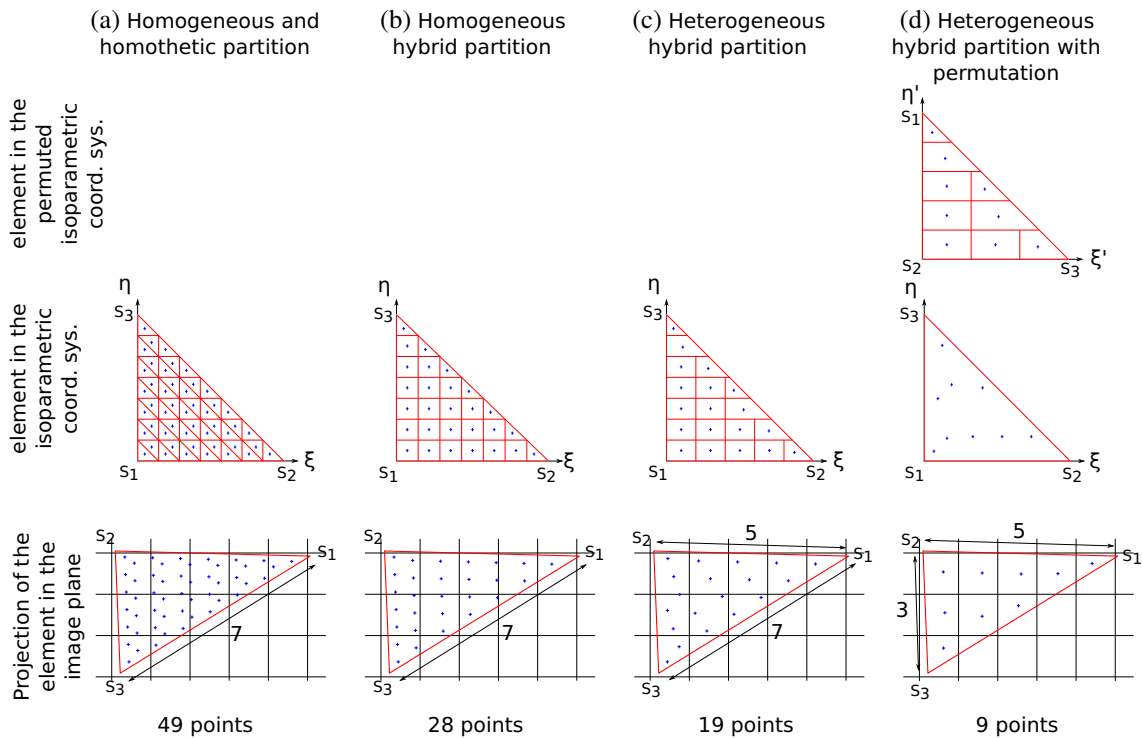
Fig. 5 Example of a different quadrature rule in the isoparametric coordinate system in order to find as few integration points as possible

top one. Here, we propose a method for measuring the mid-plane unknowns directly.

Plate kinematic regularization

With a plate theory (such as the Mindlin-Reissner theory of plates), a simple linear projector Π can be used to determine the displacement of the upper skin depending upon the displacements $\mathbf{V}$ and rotations θ of the mid-surface. By extension and for the sake of simplicity, the vector of unknowns containing displacements and rotations of the mid-surface is denoted by $\mathbf{V}$.

$$\mathbf{U} = \Pi\mathbf{V} \Leftrightarrow \begin{bmatrix} U_x \\ U_y \\ U_z \end{bmatrix} = \Pi \begin{bmatrix} V_x \\ V_y \\ V_z \\ \theta_x \\ \theta_y \end{bmatrix}$$
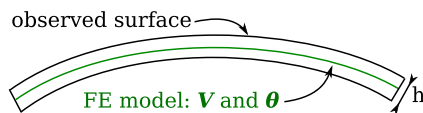
Fig. 6 Representation of a 3D plate or shell of thickness h. The 3D displacement $\mathbf{U}$ measured with an optical bench is on the observed surface whereas the plate or shell model considers displacements $\mathbf{V}$ and rotations θ at the mid-surface

Then the Stereo-DIC problem can be written:

$$\mathbf{V}^\star = \arg\min_{\mathbf{V}} \quad \frac{1 - \lambda_m}{\alpha_v} \sum_c \int_\Omega \Big[f_c\left(\mathbf{P}_c(\mathbf{X}, \mathbf{p}_c)\right)$$
$$- g_c\left(\mathbf{P}_c(\mathbf{X} + \Pi\mathbf{V}(\mathbf{X}), \mathbf{p}_c)\right) \Big]^2 d\mathbf{X}$$
$$+ \frac{\lambda_m}{\alpha_m} \|\overline{\mathbf{K}}\mathbf{V}\|_2^2 \tag{6}$$

where the unknowns are not only the displacement of the upper skin, $\mathbf{U}$, but also the five degrees of freedom, $\mathbf{V}$, of the mid-surface. α_v and α_m are weighting coefficients for vision and stiffness terms. Thus, λ_m is a dimensionless coefficient for the mechanical regularization term, set between 0 and 1 (see "Regularization coefficients"). Finally, $\overline{\mathbf{K}}$ is a regularization matrix since, when two unknowns are added per node, a regularization term is needed. Due to the formulation in the world coordinate system, the real 3D displacement is the unknown of the problem. Thus, it is easy to add a mechanical operator (such as $\mathbf{K}\mathbf{V} = \mathbf{F}$ for an elastic deformation) in order to regularize the functional. However, for the present study, it is not possible to obtain the external forces. Thus, the stiffness matrix $\mathbf{K}$ is replaced by $\overline{\mathbf{K}}$, a regularization matrix defined by $\overline{\mathbf{K}} = P_k\mathbf{K}$ with P_k a diagonal matrix (7). The latter could be Boolean but, in this study, P_k

is used to weight some *dofs* (*e.g.* to weigh the influence of rotations with respect to the membrane behaviour):

$$
\begin{cases}
P_k^{ij} = 0 & \forall j \neq i \\
P_k^{ii} = 0 & \text{for all } dofs \text{ on the non-free edges} \\
P_k^{ii} = 0 & \text{for the membrane } dofs \text{ related to } V_x \text{ and } V_y \\
P_k^{ii} = 1 & \text{for the } dofs \text{ related to } V_z \\
P_k^{ii} = \frac{1}{h^2} & \text{for the } dofs \text{ related to } \theta_x \text{ and } \theta_y \ (h \text{ being the element size})
\end{cases}
\tag{7}
$$

Thus, $\overline{\mathbf{K}}$ is a matrix containing all *dofs* except those supported by the nodes that are concerned with Dirichlet boundary conditions [20].

At iteration k, the problem reads:

$$
\underbrace{\left[\frac{1-\lambda_m}{\alpha_v} \Pi^T \mathbf{M}_{stereo}^k \, \Pi + \frac{\lambda_m}{\alpha_m} \overline{\mathbf{K}}^T \overline{\mathbf{K}} \right]}_{\mathbf{M}_{\overline{\mathbf{K}}}} \delta \mathbf{q} = \frac{1-\lambda_m}{\alpha_v} \Pi^T \mathbf{b}_{stereo}^k - \frac{\lambda_m}{\alpha_m} \overline{\mathbf{K}}^T \overline{\mathbf{K}} \, \mathbf{q}_0
$$

Remark Replacing $\mathbf{K}$ by $\overline{\mathbf{K}}$ means no regularization on the degrees of freedom of the non-free edges. Thus the behaviour of the nodes of these edges is only towed by the vision term. However, in this study, a plate model is used, which means that the unknowns are 3 displacements and 2 rotations at the mid-plate surface. An additional difficulty arises due to the fact that each *dof* on the non-free edges implies a singularity in $\mathbf{M}_{\overline{\mathbf{K}}}$. On the one hand, if these *dofs* are not taken into account, the problem cannot be solved. On the other hand, if they are removed from $\mathbf{M}_{\overline{\mathbf{K}}}$ the associated nodes are clamped. Thus, there is a difficulty, which will be solved in "Mechanical and Tikhonov regularization", especially for the rotations, as the displacement *dofs* can be considered in $\mathbf{M}_{stereo}^k$ but the rotation *dofs* cannot.

Mechanical and Tikhonov regularization

To overcome the absence of mechanical regularization on the non-free edges (particularly for rotations of these nodes in question), it is possible to add a Tikhonov regularization term (minimization of a Laplacian term):

$$
\mathbf{V}^\star = \arg\min_{\mathbf{V}} \quad \frac{1-\lambda_m-\lambda_t}{\alpha_v} \sum_c \int_\Omega \Big[f_c\left(\mathbf{P}_c(\mathbf{X}, \mathbf{p}_c)\right)
$$
$$
- g_c\left(\mathbf{P}_c(\mathbf{X} + \Pi\mathbf{V}(\mathbf{X}), \mathbf{p}_c)\right) \Big]^2 d\mathbf{X}
$$
$$
+ \frac{\lambda_m}{\alpha_m} \|\overline{\mathbf{K}}\mathbf{V}\|_2^2 + \frac{\lambda_t}{\alpha_t} \|\Delta\mathbf{V}\|_2^2
\tag{8}
$$

which gives:

$$
\left[\frac{1-\lambda_m-\lambda_t}{\alpha_v} \Pi^T \mathbf{M}_{stereo}^k \, \Pi + \frac{\lambda_m}{\alpha_m} \overline{\mathbf{K}}^T \overline{\mathbf{K}} + \frac{\lambda_t}{\alpha_t} \mathbf{T}^T \mathbf{T} \right] \delta \mathbf{q}
$$
$$
= \frac{1-\lambda_m-\lambda_t}{\alpha_v} \Pi^T \mathbf{b}_{stereo}^k - \frac{\lambda_m}{\alpha_m} \overline{\mathbf{K}}^T \overline{\mathbf{K}} \, \mathbf{q}_0 - \frac{\lambda_t}{\alpha_t} \mathbf{T}^T \mathbf{T} \, \mathbf{q}_0
$$

where $\mathbf{T}$ is the Tikhonov matrix corresponding to the Laplacian term, α_t is a weighting coefficient and λ_t is a second dimensionless coefficient for this regularization term, set between 0 and 1 with respect to λ_m (see "Regularization coefficients"). In concrete terms, each node excluded from $\mathbf{K}$ will be associated with a zero eigenvalue. Adding the Laplacian term amounts to imposing the condition that these nodes adopt a behaviour similar to that of their neighbours.

Remark The normalization coefficients α_v and α_m are computed with the initial guess of the displacement $\mathbf{U}^0$. For α_t, since any non-zero value would be appropriate, it is set to 1. The coefficients are defined by:

$$
\begin{cases}
\alpha_v = \mathbf{U}^{0^T} \mathbf{M}_{stereo}^k \mathbf{U}^0 \\
\alpha_m = \mathbf{U}^{0^T} \overline{\mathbf{K}}^T \overline{\mathbf{K}} \mathbf{U}^0 \\
\alpha_t = 1
\end{cases}
$$

Application

Synthetic test case

In order to quantify the measurement error with the regularization method described, the goal here is to create some synthetic images for a plate test case. A pair of real images taken during a test is used (Fig. 8). The plate size is $26.5 \times 26.5 \ cm^2$. Both cameras being calibrated, the two projectors $\mathbf{P}_c$ are known. On the initial plate, for each camera c, the 3D reference points of the plate $\mathbf{X}_r = (X, Y, 0)^T$ are also known. It therefore suffices to determine the displaced points (according to a plate model) corresponding to each reference point to create a new image. According to the small strain and small displacement assumption, each point originally located at position $\mathbf{X}_r = (X, Y, 0)^T$ will be moved to the point $\mathbf{X}_d = (X, Y, p(X, Y))^T$ with p a function giving the out-of-plane position of a point according to a chosen plate model. Thus, for all pixel positions $\mathbf{x}$ of the new image, two unknowns (X, Y) are sought as the solution to a system of two equations that can be solved with a Newton algorithm (Fig. 7(a)):

$$
\mathbf{P}_c((X, Y, p(X, Y))^T) - \mathbf{x} = 0
$$

Then, it is known that this displaced point was originally located at position $\mathbf{X}_r = (X, Y, 0)^T$ (Fig. 7(b)). It is thus possible to create a synthetic image of a deformed configuration by interpolating the grey-level of the reference image f_c at the pixel $\mathbf{x}$ by projecting the reference 3D point $\mathbf{P}_c(\mathbf{X}_r)$ (Fig. 7(c)).

Fig. 7 Creation of a synthetic image of a deformed configuration g_c with a plate model p. (**a**) search for the 3D displaced point $\mathbf{X}_d$ that corresponds to the pixel $\mathbf{x}$ according to a plate model p. (**b**) projection of this displaced point onto the initial shape in order to find the reference 3D point $\mathbf{X}_r$. (**c**) interpolation of the reference image to associate a grey-level with the pixel $\mathbf{x}$ of the new image g_c

(a) (b) (c)
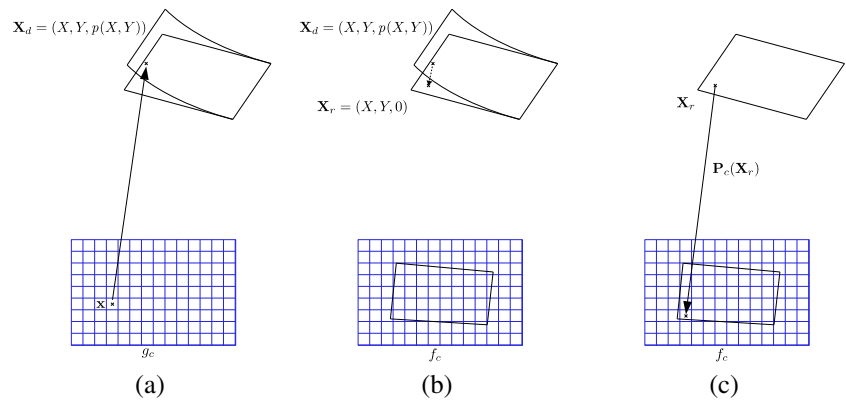
With this method, a pair of synthetic images is created for a bending plate study (Fig. 8). It is then possible to compute the measurement error by comparing the measure to the prescribed model p.

Influence of the mesh size

The idea here is to calculate the measurement error according to the mean size of the elements of an FE mesh. Both FE-SDIC and R-FE-SDIC (regularized, here with a plate model) are used. Figure 9 presents the standard deviation of the error with both methods when measuring the out-of-plane displacement V_z and the rotation θ_y. For the latter, with an FE-SDIC method, only the 3D displacement of the upper skin $\mathbf{U}$ is measured and the rotations are calculated using the derivative of the out-of-plane displacement $U_z = V_z$.

It can be seen in Fig. 9(a) that, when the mesh size decreases, the measurement error also decreases due to the "FE error" until a mean element size of approximately 10 *mm* is reached. Then, because of a lack of pixels in the projected elements, the error increases, which corresponds to the "DIC error". In contrast, it can be noted, in blue, that thanks to the mechanical regularization, the error does not increase. Figure 9(b) shows that it is possible to measure the

rotations directly, regardless of the mean element size. Also, as expected, the derivative of the measured field (in red) is noisier than the measured rotation field (in blue).

Noise robustness

It is also possible to study the behaviour of measurement uncertainties if a different level of noise is added when creating the synthetic images, cf. Fig. 10. For that purpose, we added zero-mean white Gaussian noise with an increasing standard deviation ranging from 1 to 8 grey-levels. The measurement with mechanical regularization is much more robust relative to noise.

Remarks:

– In this study, the image noise was estimated to be less than 3 grey-levels (Allied Vision Pike FireWire 5 Megapixels).

– No filtering algorithm was used in this work. The only regularisation was based on the use of a mechanical operator.
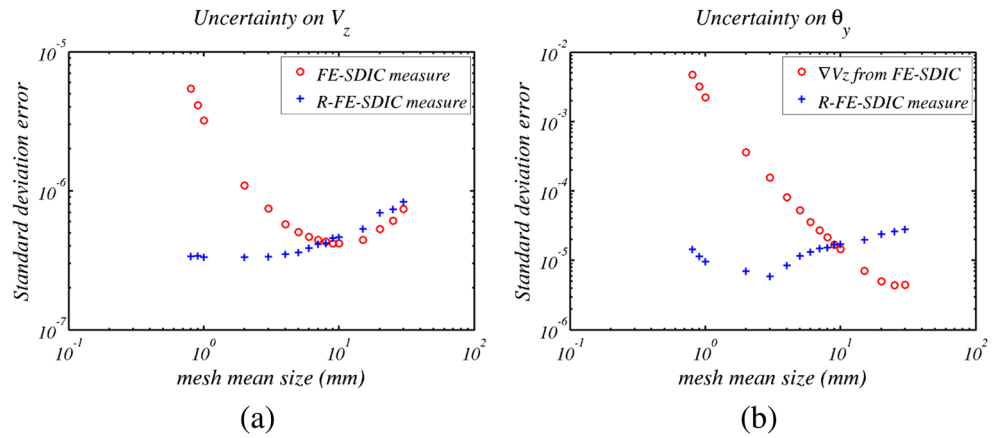
Regularization coefficients

Obviously, the result of such a measurement depends on the parameters λ_m and λ_t used. They are the cut-off wavelength

Fig. 8 Real images of a plate in bending. Reference images of *left* (**a**) and *right* (**b**) camera used to create synthetic images with a plate model p. The plate size is 26.5×26.5 *cm*^{2}
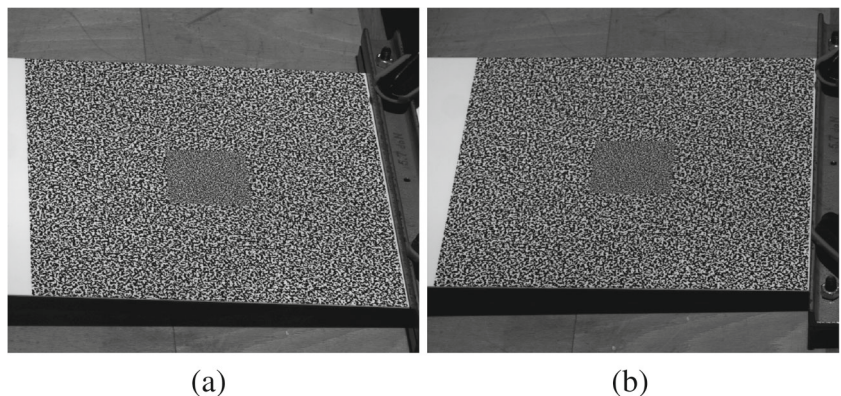
(a) (b)

of low-pass filters [8, 10, 21]. Usually, parameters of this kind are set between 0 and 1 (equation (9)). Thus, the three terms of (8) are normalized with α_v, α_m and α_t.

$$\begin{cases} 0 \le \underbrace{1 - \lambda_m - \lambda_t}_{\lambda_{vision}} \le 1 \\ 0 \le \quad \lambda_m \quad \le 1 \\ 0 \le \quad \lambda_t \quad \le 1 \end{cases} \tag{9}$$

Thus, different values of λ_m can be used in order to study the measurement error. Without mechanical regularization, a displacement can be observed but a rotation cannot. Thus, the rotation measurement with a low value of λ_m, corresponding to a low mechanical regularization, should not be less accurate than with a larger regularization coefficient. But, as can be seen in Fig. 11(a) and (c), it is hard to find the optimal parameter, especially when looking at the rotation. The simplest way to find it, for such an approach, is to draw an L-curve [7, 12] that represents both DIC and Mechanical residual. The optimal parameter will naturally be at the corner of the L-curve (cf. Fig. 11(e)).

On the other hand, the parameter λ_t aims to take account of the degrees of freedom with a Dirichlet condition. At

first view, it might seem that setting this parameter to any non-zero value would suffice: $\lambda_t \ne 0$. Yet it can be seen in Fig. 11(b), (d) and (f) that this parameter does have an impact on the measurement. In fact, the weight of this coefficient has an influence on the boundary. And since boundary displacement uncertainty has a tendency to spread in the mechanically regularized region, it has an effect on the solution [8].

Real test case

The same measurement is now carried out with real images. As expected, the measurement of the rotation by R-FE-SDIC (FE-Stereo-DIC mechanically regularized with a plate theory) is more accurate than without mechanical regularization, because the latter (FE-Stereo-DIC) is the numerical derivative of a measured field (cf. Fig. 12).

The main advantage of a Stereo method based on the world coordinate system is that it is possible to use a real mesh. In a classical FE-SDIC method, the mesh has to be adapted to the measurement. Here, the goal is to adapt the measurement in order to set up a real dialogue between experiment and simulation. The mesh chosen for a simulation can also be used for a measurement. For example, the
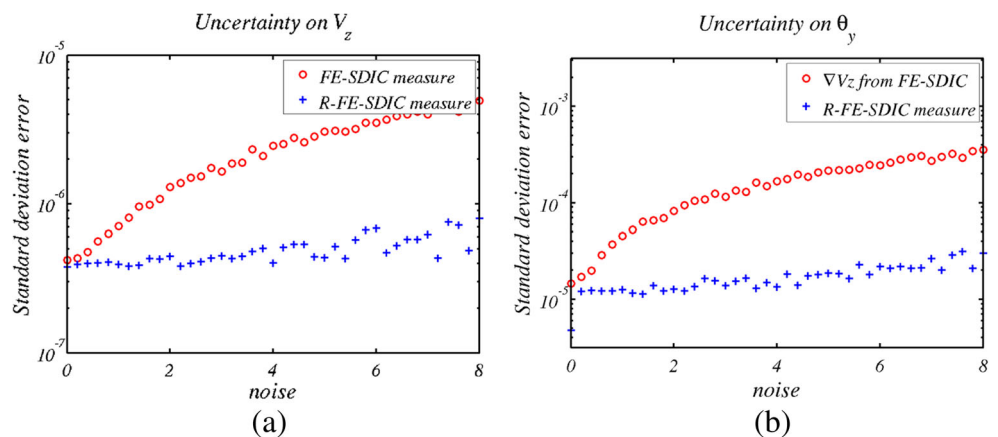
Fig. 11 Schemes for studying the influence of λ_m (*left*) and λ_t (*right*). Standard deviation of the error when measuring the out-of-plane displacement V_z (**a**, **b**) and the rotation θ_y (**c**, **d**) for different values of λ_m and λ_t. This is computed with the R-FE-SDIC measurement regularized with a plate model (*blue*) and the value corresponding to the FE-SDIC method is plotted (*red*) for comparison. L-curve (**e**, **f**) of both parameters in order to minimize both DIC and Mechanical residual
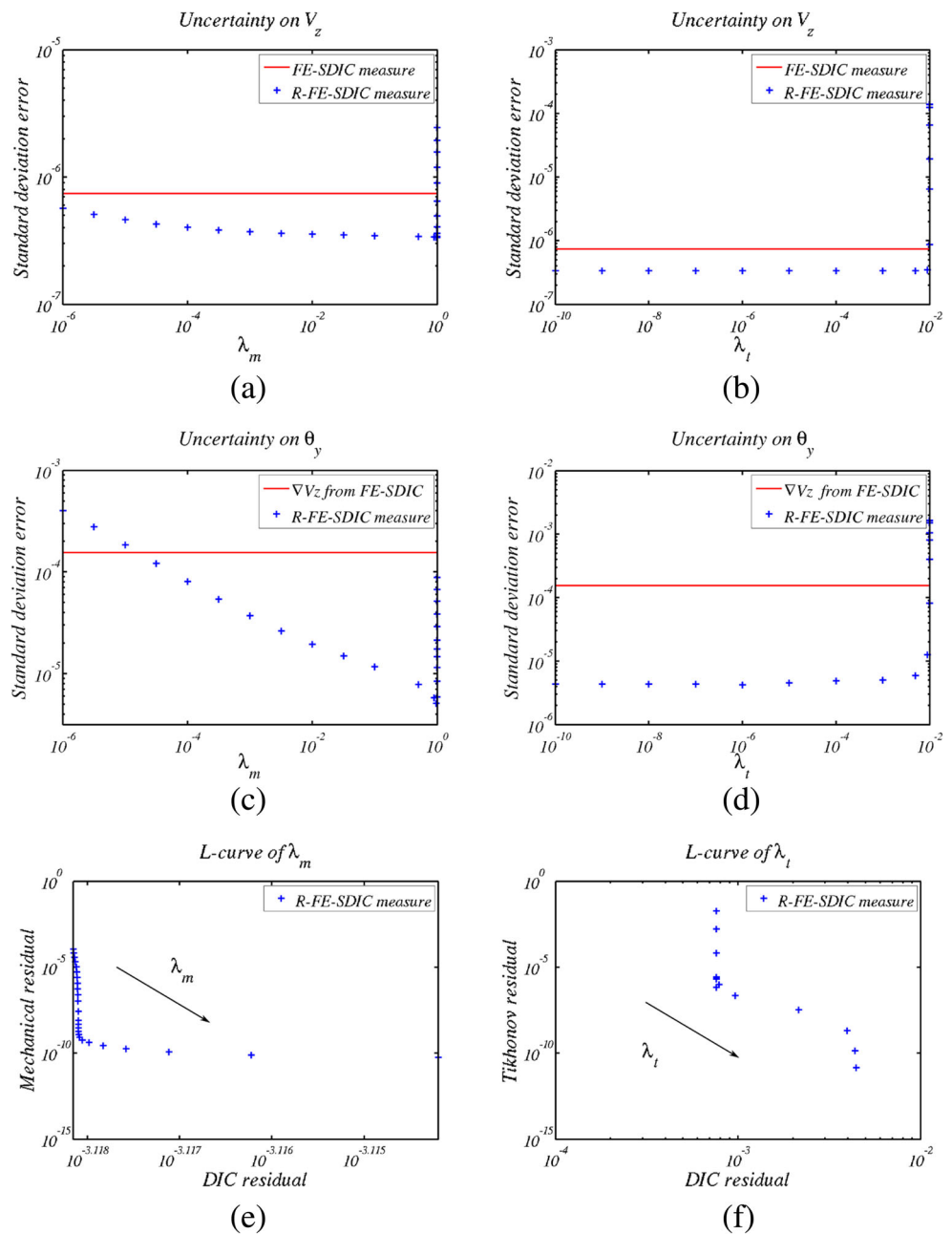
mesh can be refined in the centre for a potential defect (cf. Fig. 13). In this figure, the shape measurement is compared to the shape computed by Vic-3D$^{\text{TM}}$. It can be seen that the point cloud resulting from Vic-3D$^{\text{TM}}$ is close to the mesh except at the boundary, where the Vic-3D$^{\text{TM}}$ shape is not available.

With this kind of mesh, even the displacement field computed without regularization would not be correct because of the mesh refinement at the centre (cf. Fig. 14).

The quality of these results is verified, by looking at Vic-3D$^{\text{TM}}$ measurements of the same images sets. For example,

in Fig. 15, the out-of-plane displacement fields V_z were measured by Stereo-DIC (Vic-3D$^{\text{TM}}$) with two subset sizes (and associated steps) in order to compare the results with small or large subsets equivalent to the small and large elements of the mesh of Fig. 13.

It can be noticed that the noise level in the out-of-plane displacement measured by standard DIC code is comparable to the one measured by FE-SDIC without mechanical regularisation. In the center of the mesh where the elements are smaller, the level of noise is comparable to the one when using small subsets size. The same
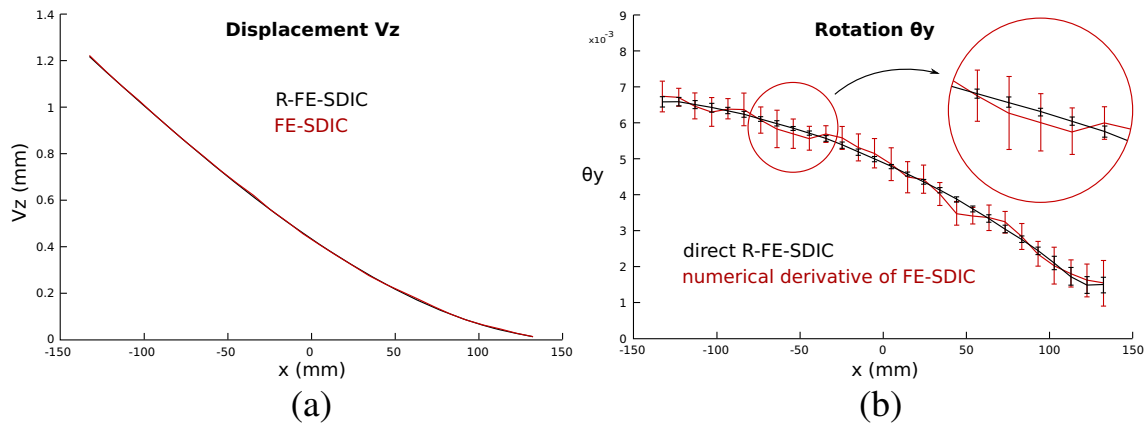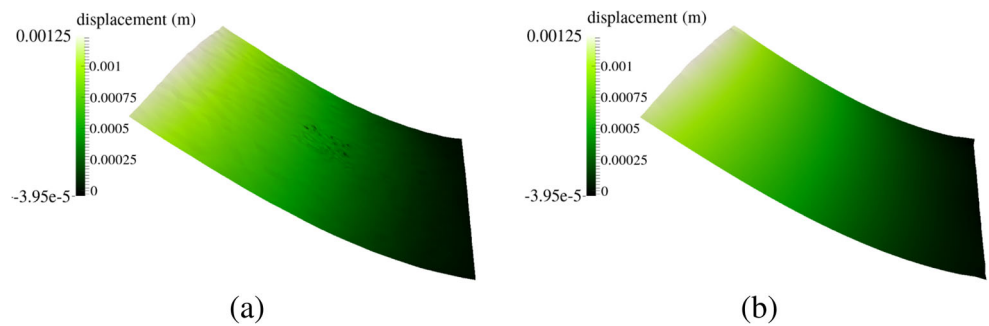
Fig. 12 Comparison of the measurement of the displacement V_z (**a**) or the rotation θ_y (**b**) with different approaches : FE-SDIC (*red*) or R-FE-SDIC (*black*)
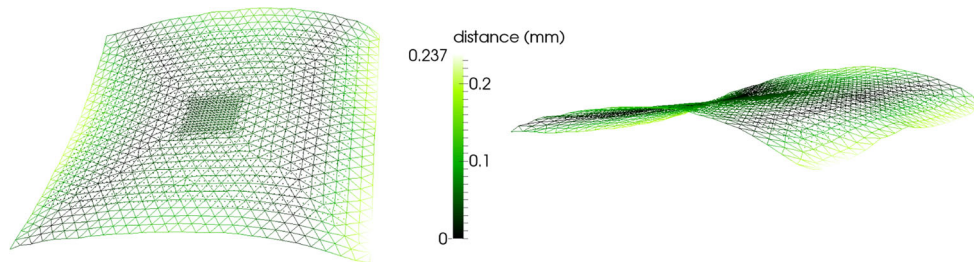

Fig. 13 Shape of a large plate measured by SDIC during an actual experiment. A suitable mesh was devised to provide a better resolved FE-SDIC measurement around a potential defect located in the centre of the plate. The FE-SDIC shape measurement (mesh) is compared to a classical SDIC shape measurement (Vic-3D^{TM}: point cloud)

Fig. 14 Comparison of the out-of-plane displacement fields V_z measured by FE-SDIC without regularization (**a**), or R-FE-SDIC with regularization (**b**)

Fig. 15 Comparison of the out-of-plane displacement fields V_z measured by Stereo-DIC (Vic-3D) with two subset sizes: (*left*) a small subset size comparable to the small elements of the mesh of Fig. 13; (*right*) a large subset size comparable to the large elements of the mesh of Fig. 13

(a) small subset size
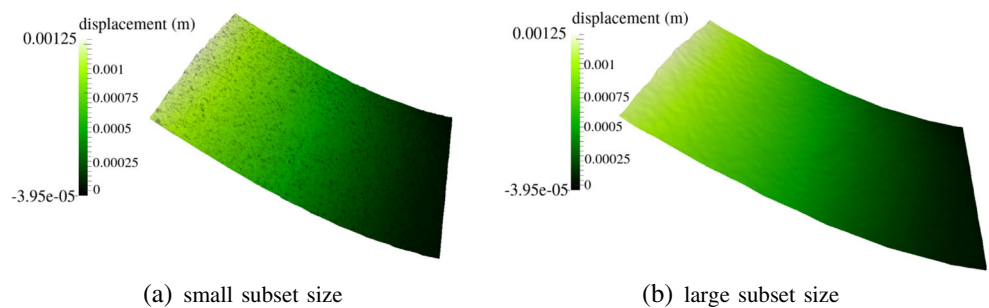
(b) large subset size

conclusion holds for larger elements and subset size. Thanks to FE-SDIC, it is possible to further regularize the measurement when using mechanical regularisation as shown in Fig. 14.

Conclusion

A full stereovision framework for measuring the 3D shape and displacements using a Finite Element mesh has been developed. The formulation incorporates a grey-level-based calibration step extended to non-linear camera models. It has been shown that, unlike stereovision using NURBS functions [1], the shape measurement is very ill-posed and requires additional regularization. For that purpose we used a type of isometric constraint. Thanks to this formulation in the world coordinate system, the same FE mesh can be shared between both numerical simulation and measurement. It is thus a good tool for performing quantitative comparisons between non-planar experiments and corresponding simulations, which are most often based on Finite Elements [26, 27]. In addition, a technique has been proposed to build the minimal number of integration points in such a context.

As an application, the method was used for the measurement of the displacement and rotation fields of a plate in bending, using a mechanical regularization based on the elastic stiffness operator associated with the FE mesh. In addition, stereo synthetic test cases were developed and analysed in order to exemplify the efficiency of the proposed method.

References

1. Beaubier B, Dufour JE, Hild F, Roux S, Lavernhe S, Lavernhe-Taillard K (2014) CAD-based calibration and shape measurement with stereoDIC: Principle and application on test and industrial parts. Exp Mech 54(3):329–341. doi:10.1007/s11340-013-9794-6

2. Besnard G, Hild F, Roux S (2006) "Finite-Element" Displacement Fields Analysis from Digital Images: Application to Portevin–Le Châtelier Bands. Exp Mech 46(6):789–803. doi:10.1007/s11340-006-9824-8

3. Dufour JE, Beaubier B, Hild F, Roux S (2015) CAD-based Displacement Measurements with Stereo-DIC: Principle and First Validations. Exp Mech. doi:10.1007/s11340-015-0065-6

4. Dufour JE, Hild F, Roux S (2015) Shape, displacement and mechanical properties from isogeometric multiview stereocorrelation. The Journal of Strain Analysis for Engineering Design. doi:10.1177/0309324715592530

5. Garcia D, Orteu JJ (2001) 3d deformation measurement using stereo-correlation applied to experimental mechanics. In: Proceedings of the 10th FIG International Symposium Deformation measurements, pp 19–22

6. Horn BKP, Schunck BG (1981) Determining optical flow. Artif Intell 17(1–3):185–203. doi:10.1016/0004-3702(81)90024-2

7. Lawson C, Hanson R (1995) Solving Least Squares Problems. Soc Ind Appl Math. doi:10.1137/1.9781611971217

8. Leclerc H, Périé JN, Hild F, Roux S (2012) Digital volume correlation: what are the limits to the spatial resolution? Mechanics & Industry 13(06):361–371

9. Leclerc H, Périé JN, Roux S, Hild F (2009) Integrated Digital Image Correlation for the Identification of Mechanical Properties. In: gagalowicz A, Philips W (eds) Computer Vision/Computer Graphics CollaborationTechniques, no. 5496 in Lecture Notes in Computer Science. Springer, Berlin Heidelberg, pp 161–171

10. Leclerc H, Périé JN, Roux S, Hild F (2011) Voxel-Scale Digital Volume Correlation. Exp Mech 51(4):479–490. doi:10.1007/s11340-010-9407-6

11. Lucas BD, Kanade T (1981) An iterative image registration technique with an application to stereo vision. In: Proceedings of Imaging Understanding workshop, pp 121–130

12. Miller K (1970) Least squares methods for ill-posed problems with a prescribed bound. SIAM J Math Anal 1(1):52–74. doi:10.1137/0501006

13. Passieux JC (2015) Quelques outils numériques pour la simulation et la mesure en mécanique des structures. Habilitation à diriger des recherches de l'université de Toulouse 122p. http://hal.archives-ouvertes.fr/tel-01370556

14. Passieux JC, Bugarin F, David C, Périé JN, Robert L (2015) Multiscale Displacement Field Measurement Using Digital Image Correlation: Application to the Identification of Elastic Properties. Exp Mech 55(1):121–137. doi:10.1007/s11340-014-9872-4

15. Passieux JC, Périé JN, Salaün M (2015) A dual domain decomposition method for finite element digital image correlation. Int J Numer Methods Eng 102(10):1670–1682. doi:10.1002/nme.4868

16. Passieux JC, Réthoré J, Gravouil A, Baietto MC (2013) Local/global non-intrusive crack propagation simulation using a multigrid X-FEM solver. Comput Mech 52(6):1381–1393. doi:10.1007/s00466-013-0882-3

17. Pierré JE, Passieux JC, Périé JN, Bugarin F, Robert L (2016) Unstructured finite element-based digital image correlation with enhanced management of quadrature and lens distortions. Opt Lasers Eng 77:44–53. doi:10.1016/j.optlaseng.2015.07.008

18. Roux S, Hild F (2006) Stress intensity factor measurements from digital image correlation: post-processing and integrated approaches. Int J Fract 140(1-4):141–157. doi:10.1007/s10704-006-6631-2

19. Roux S, Réthoré J, Hild F (2009) Digital image correlation and fracture: an advanced technique for estimating stress intensity factors of 2d and 3d cracks. J Phys D: Appl Phys 42(21):214,004. doi:10.1088/0022-3727/42/21/214004

20. Réthoré J (2010) A fully integrated noise robust strategy for the identification of constitutive laws from digital images. Int J Numer Methods Eng 84(6):631–660. doi:10.1002/nme.2908

21. Réthoré J (2015) Automatic crack tip detection and stress intensity factors estimation of curved cracks from digital images: AUTOMATIC CRACK TIP DETECTION AND SIF ESTIMATION OF CURVED CRACKS. Int J Numer Methods Eng 103(7):516–534. doi:10.1002/nme.4905

22. Réthoré J, Muhibullah, Elguedj T, Coret M, Chaudet P, Combescure A (2013) Robust identification of elasto-plastic constitutive law parameters from digital images using 3d kinematics. Int J Solids Struct 50(1):73–85. doi:10.1016/j.ijsolstr.2012.09.002

23. Sun Y, Pang JHL, Wong CK, Su F (2005) Finite element formulation for a digital image correlation method. Appl Opt 44(34):7357–7363. doi:10.1364/AO.44.007357

24. Sutton MA, Wolters WJ, Peters WH, Ranson WF, McNeill SR (1983) Determination of displacements using an improved digital correlation method. Image Vis Comput 1(3):133–139. doi:10.1016/0262-8856(83)90064-1

25. Sutton MA, Yan JH, Tiwari V, Schreier HW, Orteu JJ (2008) The effect of out-of-plane motion on 2d and 3d digital image correlation measurements. Opt Lasers Eng 46(10):746–757. doi:10.1016/j.optlaseng.2008.05.005

26. Sztefek P, Olsson R (2008) Tensile stiffness distribution in impacted composite laminates determined by an inverse method. Compos A: Appl Sci Manuf 39(8):1282–1293. doi:10.1016/j.compositesa.2007.10.005

27. Sztefek P, Olsson R (2009) Nonlinear compressive stiffness in impacted composite laminates determined by an inverse method. Compos A: Appl Sci Manuf 40(3):260–272. doi:10.1016/j.compositesa.2008.12.002

28. Triggs B, McLauchlan PF, Hartley RI, Fitzgibbon AW (2000) Bundle adjustment—a modern synthesis. In: Vision algorithms: theory and practice. Springer, pp 298–372